China Instrument and Control Society
Instrumentation
INSTRUMENTATION, Vol. 12, No. 2, June 2025
https://doi.org/10.15878/j.instr.202500245

Article

Wireless Photovoltaic Fault Monitoring System

Wenbo Xiao[1,2,3*], Huangfeng Dong[2,3], Huaming Wu[2,3], Yongbo Li[2,3], Bin Liu[2]

[1] College of Science and Technology, Nanchang Hang Kong University, Gongqing City 332020, China

[2] Key Laboratory of Nanchang Hangkong University Nondestructive Testing Technology, Ministry of Education, Jiangxi, Nanchang 330063

[3] Key Laboratory for Optoelectronic Information Perception and Instrumentation of Jiangxi Province, Nanchang Hangkong University, Nanchang 330063, China

[*] Corresponding author email 70075@nchu.edu.cn

Abstract: This study presents a wireless photovoltaic fault monitoring system integrating an STM32 microcontroller with an Improved Horned Lizard Optimization Algorithm (IHLOA) and a Multi-Layer Perceptron (MLP) neural network. The IHLOA algorithm introduces three key innovations: (1) chaotic initialization to enhance population diversity and global search capability, (2) adaptive random walk strategies to escape local optima, and (3) a cross-strategy mechanism to accelerate convergence and enhance fault detection accuracy and robustness. The system comprises both hardware and software components. The hardware includes sensors such as the BH1750 light intensity sensor, DS18B20 temperature sensor, and INA226 current and voltage sensor, all interfaced with the STM32F103C8T6 microcontroller and the ESP8266 module for wireless data transmission. The software, developed using QT Creator, incorporates an IHLOA-MLP model for fault diagnosis. The user-friendly interface facilitates intuitive monitoring and scalability for multiple systems. Experimental validation on a PV array demonstrates that the IHLOA-MLP model achieves a fault detection accuracy of 94.55%, which is 2.4% higher than the standard MLP, while reducing variance by 63.64% compared to the standard MLP. This highlights its accuracy and robustness. When compared to other optimization algorithms such as BKA-MLP (94.10% accuracy) and HLOA-MLP (94.00% accuracy), the IHLOA-MLP further reduces variance to 0.08, showcasing its superior performance. The system selects voltage as a feature vector to maintain circuit stability, avoiding efficiency impacts from series current sensors. This combined hardware and software approach further reduces false alarms to 0.1% through a consecutive-judgment mechanism, significantly enhancing practical reliability. This work provides a cost-effective and scalable solution for improving the stability and safety of PV systems in real-world applications.

Keywords: STM32; horned lizard optimization algorithm; multilayer perceptron; fault diagnosis; photovoltaic monitoring

Citation: Wenbo Xiao, Huangfeng Dong, Huaming Wu, Yongbo Li, Bin Liu. "Wireless Photovoltaic Fault Monitoring System. " Instrumentation 12, no.2 (June 2025). https://doi.org/10.15878/j.instr.202500245

1 Introduction

Machine learning-based photovoltaic fault detection systems have been widely applied [1]. Common machine learning algorithms include Fuzzy C-means clustering, Support Vector Machines, and Artificial Neural Networks (ANN) [2-4]. The parameters of the ANN model, such as weight vectors and bias vectors, play a decisive role in the final results, hence optimizing these parameters can lead to better performance[5]. In this regard, Mohamed utilized the Genetic Algorithm (GA) for structural optimization of the ANN model, surpassing the performance of traditional ANN models and achieving an average accuracy rate of 97.63% for different fault

detections[6]. Eldeghady employed the Particle Swarm Optimization (PSO) algorithm to optimize the Backpropagation Neural Network (BPNN), combining the local search capability of BPNN with the global search capability of PSO. Compared to traditional BPNN, this model showed an 8% increase in accuracy [7]. Yu et al. used the improved Ant Colony Algorithm (ACA) to optimize the center and width of the Radial Basis Function Neural Network (RBFNN). The RBFNN optimized by ACA is characterized by fast convergence and high diagnostic accuracy [8]. From this perspective, machine learning algorithms have made significant strides in photovoltaic fault detection systems, with diverse techniques employed to enhance diagnostic accuracy. However, practical implementation faces numerous hurdles, such as fluctuating environmental conditions, the intricate nature of photovoltaic systems, varied fault categories, and the substantial computational overhead of machine learning models. Furthermore, these algorithms commonly grapple with limitations like susceptibility to local optima, sluggish convergence rates, performance sensitivity to parameter tuning, and diminished exploration capabilities during iterative optimization[9].

To address these issues, this paper adopts an improved Horned Lizard Optimization Algorithm (IHLOA) with chaotic mapping, random walk, and cross-strategy to optimize the weight vector and bias vector of the MLP. The algorithm is compared with other algorithms such as the Artificial Protozoa Optimizer (APO) [10], Bitterling Fish Optimization (BFO) [11], Partial Reinforcement Optimizer (PRO) [12], Horned Lizard Optimization Algorithm (HLOA) [13], Hippopotamus Optimization Algorithm (HO) [14], Lungs Performance-Based Optimization (LPO) [15], Electric Eel Foraging Optimization (EEFO) [16], Love Evolution Algorithm (LEA) [17], Newton-Raphson-Based Optimizer (NRBO) [18], Football Team Training Algorithm (FTTA) [19], Black-winged Kite Algorithm (BKA) [20], and Goose Optimizer (GO) [21]. Additionally, a data acquisition subsystem is constructed and the collected data is transmitted to the upper computer. The IHLOA-MLP model is loaded onto the upper computer, and the transmitted data is used for photovoltaic fault monitoring, thereby establishing a wireless photovoltaic fault detection system.

2 Fault Diagnosis Model

2.1 Multi-Layer Perceptron (MLP)

The MLP is a neural network architecture comprising an input layer, multiple hidden layers, and an output layer, where neurons in each layer establish full connections with all neurons in adjacent layers [22]. The nonlinear processing capability of MLP stems from its utilization of nonlinear activation functions in each neuron, enabling effective resolution of complex pattern recognition tasks. However, MLP performance exhibits critical sensitivity to parameter configurations, particularly weight initialization and bias optimization. To mitigate this limitation, this study introduces the Improved Horned Lizard Optimization Algorithm (IHLOA) for systematic parameter tuning. The MLP model constructed in this paper consists of two hidden layers with 10 and 15 neurons, respectively.

2.2 Horned Lizard Optimization Algorithm (HLOA)

The HLOA is a metaheuristic optimization algorithm that simulates the survival strategies of horned lizards, proposed by Peraza in 2024. Its inspiration comes from the biological behaviors that horned lizards adopt when facing predators, including hiding, skin color change, blood squirting, and escape strategies. When threatened, horned lizards integrate with their surroundings to evade predators, making them difficult to detect. Another defensive strategy is to flee, and additionally, when threatened, these lizards will adopt aggressive strategies, such as expelling a short burst of blood over a meter away. Furthermore, horned lizards can lighten or darken their skin to better conceal themselves.

2.3 IHLOA -MLP

To enhance the performance of the HLOA, this paper employs logistic chaotic mapping [23], random walk strategy [24], and cross-elbow strategy [25] to optimize the Horned Lizard Algorithm, resulting in the IHLOA.

The IHLOA is used to optimize the weight vector and bias vector of the MLP, thereby obtaining the "optimal" MLP model, as shown in Fig. 1. The specific process of this algorithm is as follows:

1. Set the basic parameters for the MLP and the algorithm: the number of neurons in the input layer of the MLP (determined by the dataset), the number of neurons in the hidden layer (2 hidden layers with 15 and 20 neurons respectively), the number of neurons in the output layer (1), the number of iterations (500), the population size of the optimization algorithm (set to 50), the dimension of the individual (determined by the dataset), and the maximum number of iterations (200).

2. Initialize the weight vector and bias vector.

3. Use a chaotic algorithm to initialize the population individuals.

4. Calculate the fitness value of the population individuals through the objective function, and determine the current optimal value.

5. Determine if the fitness value has not changed for 5 consecutive times; if so, introduce a random walk to update the individual's position and jump to step (9).

6. Decide whether a color change is needed; if yes, update the individual's position and jump to step (8); if not, then decide whether to escape.

7. Determine whether to escape, thereby updating the individual's position.

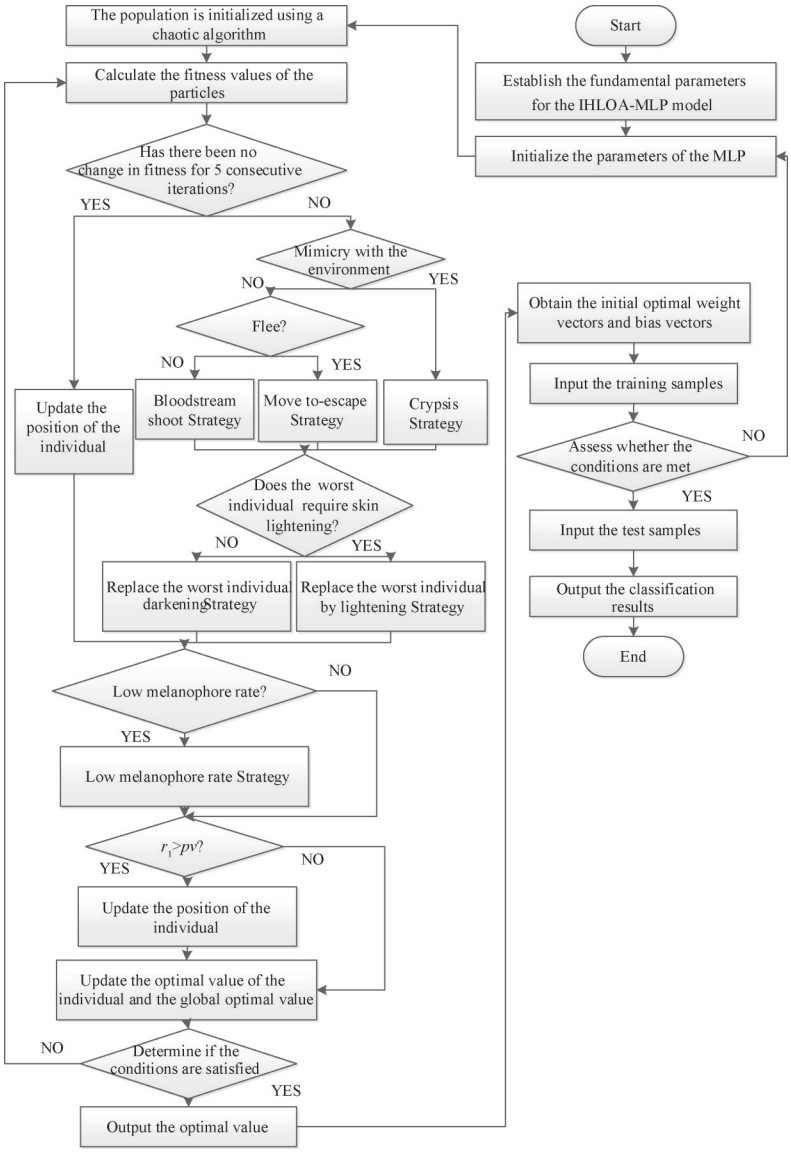

Fig.1 IHLOA -MLP flow chart

8. Determine if there is a need to change the skin brightness, thereby updating the individual's position.

9. Determine if the melanin cell ratio is less than 0.3; if so, update the individual's position.

10. Determine if $r_1 > pv$, where r_1 is a random number; if yes, then introduce the cross-matrix strategy and update the individual.

11. Update the position of the population individuals, calculate their respective fitness values, and update the optimal value.

12. Determine if the termination condition of the algorithm is met. If the algorithm reaches the maximum number of iterations or the precision requirement, then end and output the extreme value; otherwise, go to step (4) to continue the iteration.

13. Use the optimal values obtained from the algorithm to set the parameters of the MLP and perform performance evaluation.

2.4 Key Formulas for IHLOA

To enhance the performance of HLOA, the logistic chaotic mapping, random walk strategy, and crossover strategy are used, resulting in an Improved Horned Lizard Optimization Algorithm (IHLOA).

2.4.1 Logistic Chaos Mapping

The logistic chaos mapping is utilized to initialize the population distribution, thereby increasing the diversity of the population's search. The formula for the logistic chaos mapping is as follows:

$$X_{n+1} = r \times X_n \times (1 - X_n) \tag{1}$$

Where, $X_n \in [0, 1], n \in [0, N]$.

2.4.2 Random Walk Strategy

To enhance the search capability of the algorithm, a random walk strategy is introduced. The random walk process can be represented by Equation (2).

$$X(t)=\{0, c_{ussum}[2r(t_1)-1], c_{ussum}[2r(t_2)-1], \ldots, c_{ussum}[2r(t_n)-1],\} \quad (2)$$

$$r(t)=\begin{cases}1, & rand>0.5\\ 0, & rand\le 0.5\end{cases} \quad (3)$$

Where $X(t)$ denotes the set of step sizes for the random walk process; c_{ussum}represents the cumulative sum of the step counts in the random walk process; t is the current step count in the random walk process; t_n represents the step count for the n instance of the random walk. $r(t)$ is a random number uniformly distributed in the interval [0, 1].

2.4.3 Crossover Strategy

To prevent premature maturation of horned lizard individuals, a crisscross strategy is used to enhance the global search ability.

2.4.3.1 Horizontal Crossover

Horizontal crossover is an algorithmic technique that operates between two distinct horned lizards, facilitating arithmetic crossover across all dimensions to encourage mutual learning among these individuals and enhance the overall search capability. Initially, each individual is randomly paired, serving as parents. After the parent matching, offspring are obtained through Equations (4) and (5).

$$MS_{hc}^{i_1 j}=r_1\times MS_{i_1 j}+(1-r_1)\times MS_{i_2 j}+c_1\times(MS_{i_1 j}-MS_{i_2 j}) \quad (4)$$

$$MS_{hc}^{i_2 j}=r_2\times MS_{i_2 j}+(1-r_2)\times MS_{i_1 j}+c_2\times(MS_{i_2 j}-MS_{i_1 j}) \quad (5)$$

Where $MS_{i_1 j}$ and $MS_{i_2 j}$ represent the j dimensional data of parent MS_{i_1} and parent MS_{i_2}, respectively; $MS_{hc}^{i_1 j}$ and $MS_{hc}^{i_2 j}$ represent the j dimensional data of the offspring produced by horizontal crossover; r_1 and r_2 are a random variable uniformly distributed on the open interval (0, 1); c_1 and c_2 are a random variable uniformly distributed on the open interval (-1, 1). The offspring generated engage in competition with their parental counterparts, with the ultimate retention of the more advantageous individuals.

2.4.3.2 Vertical crossover

Vertical crossover is an algorithmic technique that operates among all horned lizard individuals, performing arithmetic crossover on two distinct dimensions. Additionally, vertical crossover generates only one offspring at a time, avoiding the disruption of other dimensions that might represent optimal solutions, while also providing opportunities for stagnant dimensions to escape from local optima. The offspring individual is obtained through vertical crossover as described by Equation (6).

$$MS_{vc}^{ij_1}=k\times MS_{ij_1}+(1-k)\times MS_{ij_2} \quad (6)$$

Where MS_{ij_1} and MS_{ij_2} represent the $j_1$and j_2 dimensional data of parents MS_{ij}, respectively; k is uniformly distributed on the interval (0,1); $MS_{vc}^{ij_1}$ is the data obtained from the vertical crossover of parent MS_{ij} at the j_1 and j_2 dimensions. Similarly, the offspring generated are subjected to competition with their parents, with the fittest individuals being ultimately retained.

The definition of pv is given by Equation (7).

$$pv=\frac{2\times\left(1-\left(\frac{t}{Max\_iter}\right)^{1.5}\right)}{3} \quad (7)$$

Where Max_iter represents the maximum number of iterations allowed in the algorithm; t denotes the current iteration number within the algorithmic process. Concurrently, a random number r is generated, uniformly distributed on the interval (0, 1).

The IHLOA-MLP pseudocode is as follows:

```
IHLOA-MLP pseudo-code
Initialize IHLOA parameters: population size (P), maximum iterations (T_max), dimension (D)
Initialize MLP parameters: learning rate (eta), number of epochs (E), number of hidden layers (L), number of neurons in each layer (H)
Initialize population using logistic chaotic map
  for i = 1 to P
    x_i = logistic_chaos_map(mu, D)
Evaluate fitness of initial population
  for i = 1 to P
    Initialize MLP with weights and biases from x_i
    Train MLP for E epochs
    Evaluate fitness_i = f(x_i)
  While t < T_max
    for i = 1 to P
      if no change in fitness for 5 consecutive iterations
        if mimicry with environment
          update position of individuals using environment mimicry strategy
        elseif flee
          update position of individuals using move-to escape strategy
        else
          update position of individuals using bloodstream shoot strategy
      if worst individual requires skin lightening
          update position of individuals using lightening strategy else
          update position of individuals using darking strategy
      if low melanophore rate
        x_i =x_i+rand()*(x_i-x_prev)
      if fitness has not changed for T consecutive iterations
        x_i = x_i + sigma * randn(D)  // Random walk strategy
      else if color change is needed
        x_i = x_i + alpha * (x_best-x_i)  // Horizontal crossover
      else if escape is needed
        x_i = x_i + beta * (x_best-x_i)  // Vertical crossover
      else if skin brightness change is needed
        x_i = x_i + gamma * (x_best-x_i)  // Additional
exploration strategy
    Ensure the updated positions are within bounds
      for d = 1 to D
        if x_i[d] < x_min[d]
            x_i[d] = x_min[d]
          else if x_i[d] > x_max[d]
            x_i[d] = x_max[d]
    Initialize MLP with weights and biases from x_i
        Train MLP for E epochs
        Evaluate fitness_i = f(x_i)
        if fitness_i < fitness_best
          x_best = x_i
          fitness_best = fitness_i
      Increment t
  End While
  Return x_best  // Optimal weights and biases for MLP
End
```

Fig.2 IHLOA -MLP pseudo-code

3 System Composition

To address the common challenges of local optima convergence and environmental interference-induced false alarms in photovoltaic monitoring, this section systematically elucidates the co-design objectives of the hardware sensing unit and the IHLOA-MLP algorithm architecture.

3.1 Hardware System

The hardware of this system mainly consists of an STM32 minimum system (power supply circuit, reset circuit, clock circuit, debug circuit), BH1750 (light intensity sensor), DS18B20 (temperature sensor), Maximum Power Point Tracking (MPPT) module, battery pack, ESP8266 (WIFI module), and INA226 (current and voltage sensor). The BH1750, INA226, and DS18B20 respectively collect current light intensity data, array output current and voltage values, and temperature data, and send them to the STM32. The STM32 communicates with the upper computer through the ESP8266 for data transmission. The MPPT module steps down the array output voltage and charges the battery pack. The system schematic is shown in Figure 1-1. The detailed information on the sensor hardware can be seen in Figure 1-2 and Table 1, and the overall system is shown in Figure 1-3.

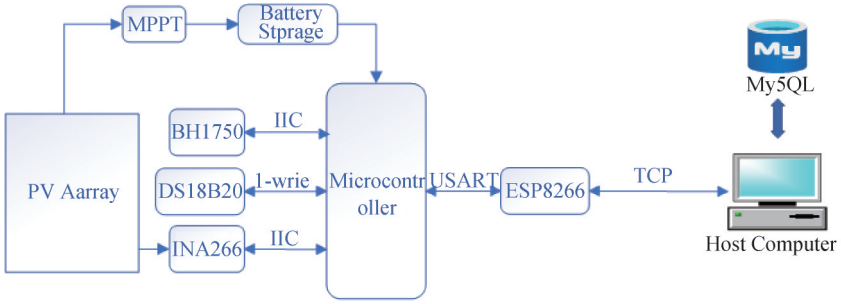

(1) Schematic diagram of the system

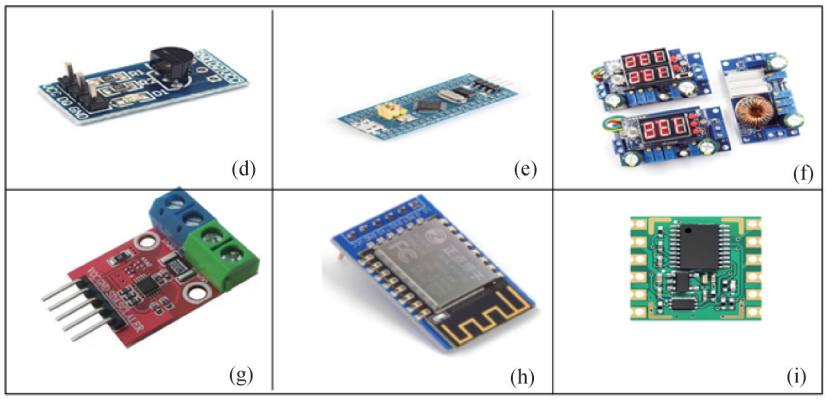

(d) DS18B20; (e) STM32; (f) MPPT; (g) INA226; (h) ESP8266; (i) BH1750

(2) Related har dware module

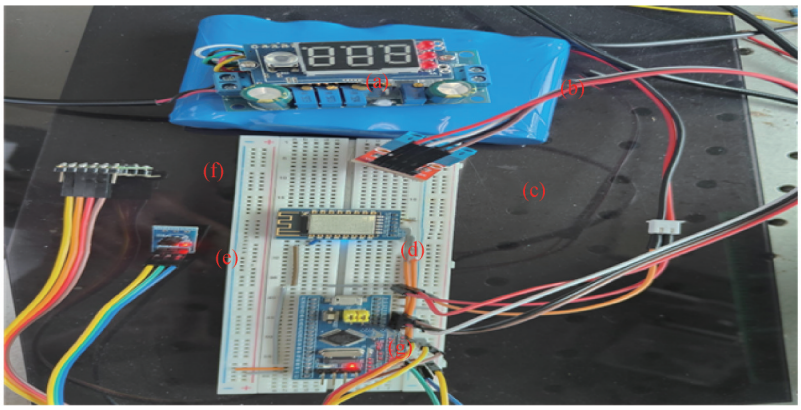

(a) Mppt; (b) Stprage batteries; (c) INA226; (d) ESP8266; (e) DSO8B20; (f)BH1750; (g) STM32

(3) Overall system diagram

Fig.3 System diagram

Table 1 Sensor parameters

Sensor	Measurement range	Operating voltage	Accuracy
ESP8266	None	5V	None
DS18B20	-55°~125°	3~5 V	±2°
BH1750	0~65535 lx	3~5 V	±1 lx
INA226	Voltage: 0~36 V	2.7~5.5 V	±1 %

3.2 Software System

The system is developed in QT Creator with an MLP neural network from OpenCV for monitoring. When the upper computer starts, it shows the connection status with the lower computer. By adjusting parameter buttons, users can visualize voltage, light intensity, and temperature in the QChart module. After the IHLOA-MLP model classifies the data, the fault type and indicator light display the results. Once a threshold is reached, data including time, system number, voltage, temperature, light intensity, and fault type are stored in a MySQL database, which users can review via the historical records button. Monitoring interface of system can be seen in Figure 4.

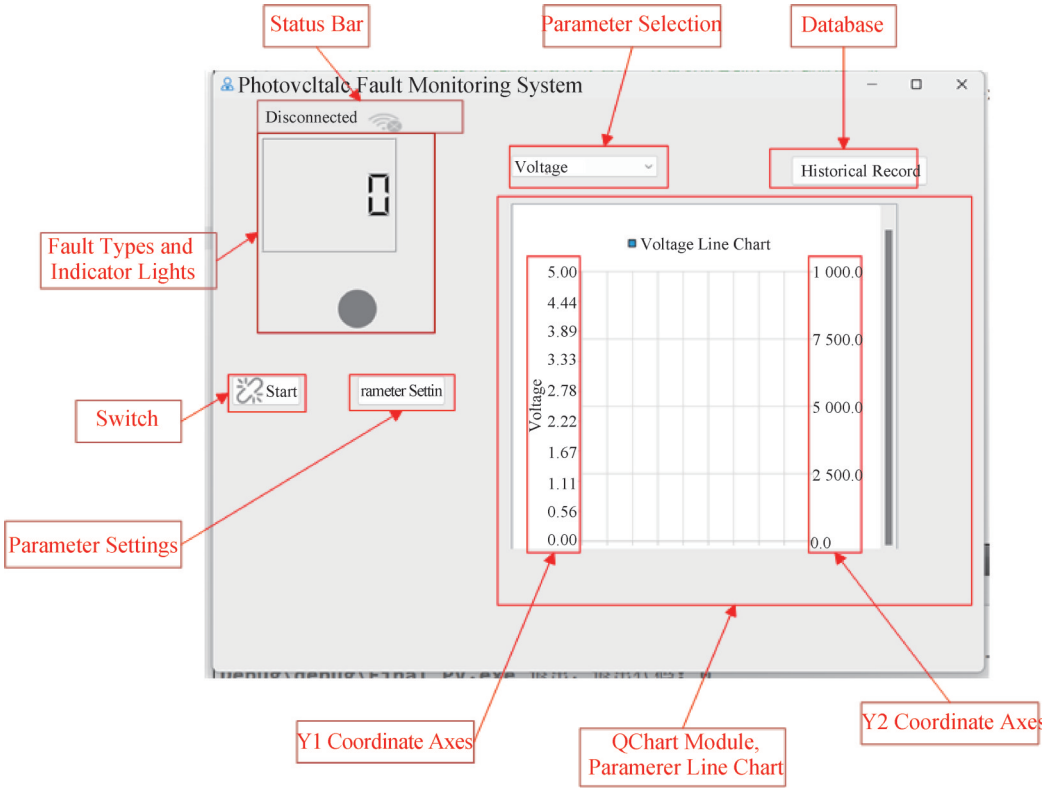

Fig.4 Monitoring interface of system

The system requires configuration of the judgment count N for updating the fault data after N consecutive same judgments, the storage interval count M for storing and plotting data every M judgments, the maximum values of y1 and y2 for the QChart axes, the maximum storage count for the database with automatic deletion of the oldest ten entries when exceeded, and the command sending interval T for generating a timeout signal every T seconds to request data.

The system is capable of indicating whether a fault has occurred in the monitored system through the fault type and indicator light module, and it can also trigger an alarm. The QChart module displays real-time monitoring data (such as current and voltage) and plots line charts. The monitoring data and judgment results are stored in a database for subsequent review.

4 Validate the fault monitoring model with experimental data

To validate the performance of the proposed algorithm, a 3×3 series-parallel combined photovoltaic array was constructed, shown in Figure 5. The 3×3 series-parallel experimental solar cell's framework is also adopted in the literature[26,27]. The photovoltaic array consists of 9 identical cells. To optimize circuit performance and protect the cells, shunt bypass diodes are incorporated in the design. This setup forms a comprehensive experimental solar cell system framework. With such a design, it can not only simulate actual photovoltaic energy conversion scenarios but also facilitate in-depth analysis and discussion of various characteristics and issues in the photovoltaic power

generation process. In the experiment, acrylic boards were used to simulate shading faults, individual or multiple route wires were disconnected to simulate open-circuit faults, and two batteries were connected with a wire to simulate short-circuit faults. A total of 400 sets of data were collected, including 100 sets of normal operation data, 100 sets of shading fault data, 100 sets of open-circuit fault data, and 100 sets of short-circuit fault data. The feature vectors included voltage, current, temperature, and light intensity. In this paper, the number of particle swarm individuals in the optimization algorithm was set to 50, and the algorithm was iterated 200 times, with the training data and test data divided into a 7∶3 ratio. At the same time, to better judge the recognition effect of the algorithm, the average recognition accuracy and its variance over 20 trials were chosen as the evaluation metrics for the model.

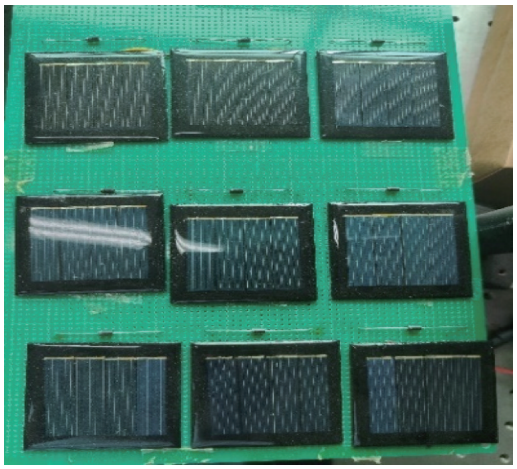

Fig.5 3×3 photovoltaic array

In fact, all the optimization algorithms compared in the table are configured with the same parameters, such as the particle population is 50 and the iteration is 200 times. In addition, the initialization parameters of each algorithm are taken directly from the optimal parameter values of the original literature. For example, the skin brightness threshold of HLOA is set at 0.3, the electric field intensity of EEFO is maintained at 2.0 kV/m, and the subduction Angle of BKA is fixed at 45° . For dynamic parameters (such as the lung capacity decay rate of LPO and the strengthening rate of PRO), the adaptive adjustment mechanism described in the literature is strictly followed. This configuration strategy ensures that the characteristics of the algorithm are fully preserved in the comparison experiment, and the performance bias caused by parameter tuning is eliminated.

4.1 Model Validation under Variations of Input Parameters

4.1.1 Current, voltage, temperature, and light intensity are utilized as input variables

Fourteen algorithms were used to identify a dataset that includes features such as current, voltage, temperature, and light intensity. The results are shown in Table 2. The IHLOA-MLP had the best recognition effect, with an average accuracy of 94.55%, while the HO-MLP and FTTA-MLP had the worst recognition effects, with an average accuracy of only 90.90%. In terms of stability, the IHLOA-MLP is not only highly accurate but also the most stable among the 14 optimization algorithms, with the smallest variance. The ranking of the algorithms from highest to lowest accuracy is as follows: IHLOA-MLP, BKA-MLP, GO-MLP, APO-MLP, BFO-MLP, PRO-MLP, LPO-MLP, EEFO-MLP, LEA-MLP, NRBO-MLP, HLOA-MLP, HO-MLP, FTTA-MLP, MLP. The ranking from lowest to highest variance is: IHLOA-MLP, BKA-MLP, APO-MLP, BFO-MLP, PRO-MLP, LPO-MLP, HLOA-MLP, EEFO-MLP, LEA-MLP, NRBO-MLP, HO-MLP, FTTA-MLP, MLP. The most unstable algorithm is the HO-MLP, with a variance of 0.62.

Table 2 Average recognition effect of each algorithm in data set with current, voltage, temperature and light intensity as input

Algorithm	Accuracy(%)	Accuracy Variance
MLP[12]	92.15	0.22
APO-MLP[10]	91.50	0.61
IHLOA -MLP	94.55	0.08
BFO-MLP[11]	91.60	0.27
PRO-MLP[12]	91.70	0.44
HLOA-MLP[13]	94.00	0.17
HO-MLP[14]	90.90	0.62
LPO-MLP[15]	92.50	0.18
EEFO-MLP[16]	91.40	0.51
LEA-MLP[17]	91.20	0.38
NRBO-MLP[18]	91.50	0.47
FTTA-MLP[19]	90.90	0.26
BKA-MLP[20]	94.10	0.12
GO-MLP[21]	92.30	0.32

From Table 2, it can be observed that the IHLOA-MLP algorithm has improved accuracy compared to the other 13 algorithms. Specifically, the accuracy has been enhanced by 2.4% over the traditional MLP algorithm and by 0.55% compared to the HLOA-MLP algorithm. Additionally, the IHLOA-MLP exhibits the smallest variance, which is only 0.08, indicating a more stable system. When compared to other optimization algorithms, the IHLOA-MLP continues to demonstrate the best performance, with the highest accuracy and the lowest variance, thus offering the best robustness.

4.1.2 Voltage, current, and light intensity are utilized as the input variables

The recognition results of the 14 algorithms on the dataset with feature vectors of voltage, current, and light intensity are shown in Table 3. It can be observed that the IHLOA-MLP algorithm has the best recognition effect, with an average accuracy of 86.40%, while the MLP algorithm has the worst recognition effect, with only 81.70%. In terms of stability, the IHLOA-MLP is not only highly accurate but also the most stable among the 14 optimization algorithms, with the smallest variance. The ranking of the algorithms from highest to lowest accuracy is as follows: IHLOA-MLP, BFO-MLP, APO-MLP, PRO-MLP, HLOA-MLP, HO-MLP, LPO-MLP, EEFO-MLP, LEA-MLP, NRBO-MLP, FTTA-MLP, BKA-MLP, MLP. The ranking from lowest to highest variance is: IHLOA-MLP, BFO-MLP, APO-MLP, PRO-MLP, HLOA-MLP, LPO-MLP, HO-MLP, EEFO-MLP, LEA-MLP, NRBO-MLP, FTTA-MLP, BKA-MLP, MLP. The most unstable algorithm is the PRO-MLP, with a variance of 0.60.

Table 3 Average recognition effect of each algorithm in the data set with voltage, current and light intensity as input

Algorithm	Accuracy(%)	Accuracy Variance
MLP[12]	81.70	0.67
APO-MLP[10]	84.70	0.51
IHLOA-MLP	86.40	0.41
BFO-MLP[11]	84.80	0.41
PRO-MLP[12]	83.90	0.60
HLOA-MLP[13]	83.20	0.43
HO-MLP[14]	83.50	0.43
LPO-MLP[15]	82.50	0.43
EEFO-MLP[16]	82.80	0.49
LEA-MLP[17]	82.60	0.41
NRBO-MLP[18]	82.80	0.43
FTTA-MLP[19]	82.40	0.41
BKA-MLP[20]	82.00	0.48
GO-MLP[21]	82.70	0.42

From Table 3, it is evident that the IHLOA-MLP algorithm continues to outperform the other 13 optimization algorithms, with the highest accuracy. Specifically, the accuracy of IHLOA-MLP is 4.7% higher than that of the MLP algorithm and 1.2% higher than that of the HLOA-MLP algorithm. Additionally, IHLOA-MLP has the smallest variance, indicating the best robustness. When compared to the dataset with feature vectors of current, voltage, temperature, and light intensity, the algorithm that is most affected among the 14 optimization algorithms is the BKA-MLP, with a decrease in accuracy of 12.1%. The algorithms least affected are the APO-MLP and BFO-MLP, with a decrease in accuracy of 6.8%, and the IHLOA-MLP has a decrease in accuracy of 8.15%.

4.1.3 Current, temperature, and light intensity are utilized as the input variables

The recognition results of the 14 algorithms on the dataset with feature vectors of current, temperature, and light intensity are shown in Table 4. It can be observed that the IHLOA-MLP algorithm has the best recognition effect, with an average accuracy of 91.80%, while the MLP algorithm has the worst recognition effect, with only 85.80%. In terms of stability, the IHLOA-MLP is not only highly accurate but also the most stable among the 14 optimization algorithms, with the smallest variance. The ranking of the algorithms from highest to lowest accuracy is as follows: IHLOA-MLP, APO-MLP, LPO-MLP, BFO-MLP, PRO-MLP, HLOA-MLP, HO-MLP, LEA-MLP, NRBO-MLP, EEFO-MLP, FTTA-MLP, BKA-MLP, MLP. The ranking from lowest to highest variance is: IHLOA-MLP, APO-MLP, BFO-MLP, PRO-MLP, HLOA-MLP, LEA-MLP, LPO-MLP, GO-MLP, EEFO-MLP, HO-MLP, FTTA-MLP, MLP. The most unstable algorithm is the EEFO-MLP, with a variance of 0.89.

Table 4 Average recognition effect of each algorithm in data set with current, temperature and light intensity as input

Algorithm	Accuracy(%)	Accuracy Variance
MLP[12]	85.80	0.82
APO-MLP[10]	90.20	0.27
IHLOA-MLP	91.80	0.19
BFO-MLP[11]	88.20	0.60
PRO-MLP[12]	89.70	0.37
HLOA-MLP[13]	89.10	0.38
HO-MLP[14]	88.10	0.76
LPO-MLP[15]	90.20	0.39
EEFO-MLP[16]	86.80	0.89
LEA-MLP[17]	89.90	0.26
NRBO-MLP[18]	90.90	0.52
FTTA-MLP[19]	86.50	0.43
BKA-MLP[20]	89.40	0.50
GO-MLP[21]	90.40	0.43

From Table 4, it is evident that the IHLOA-MLP algorithm continues to outperform the other 13 optimization algorithms, with the highest accuracy. Specifically, the accuracy of IHLOA-MLP is 6% higher than that of the MLP algorithm and 2.7% higher than that of the HLOA-MLP algorithm. Additionally, IHLOA-MLP

has the smallest variance, indicating the best robustness. When compared to the dataset with feature vectors of current, voltage, temperature, and light intensity, the algorithm that is most affected among the 14 optimization algorithms is the MLP, with a decrease in accuracy of 6.35%. The algorithm least affected is the NRBO-MLP, with a decrease in accuracy of 0.6%, and the IHLOA-MLP has a decrease in accuracy of 2.75%.

4.1.4 Voltage, temperature, and light intensity are utilized as the input variables

From Table 5, it is evident that the IHLOA-MLP algorithm continues to outperform the other 13 optimization algorithms, with the highest accuracy. Specifically, the accuracy of IHLOA-MLP is 92.20%, which is 2.6% higher than that of the MLP algorithm. Additionally, IHLOA-MLP has the smallest variance, indicating the best robustness. The ranking of the algorithms from highest to lowest accuracy is as follows: IHLOA-MLP, BFO-MLP, PRO-MLP, HLOA-MLP, LPO-MLP, NRBO-MLP, EEFO-MLP, LEA-MLP, HO-MLP, FTTA-MLP, BKA-MLP, GO-MLP, MLP. The ranking from lowest to highest variance is: IHLOA-MLP, BFO-MLP, PRO-MLP, HLOA-MLP, LPO-MLP, NRBO-MLP, EEFO-MLP, LEA-MLP, HO-MLP, FTTA-MLP, BKA-MLP, GO-MLP, MLP. The most unstable algorithm is the FTTA-MLP, with a variance of 0.71.

Table 5 Average recognition effect of each algorithm in the value data set with voltage, temperature and light intensity as input

Algorithm	Accuracy(%)	Accuracy Variance
MLP[12]	89.60	0.28
APO-MLP[10]	90.60	0.40
IHLOA-MLP	92.20	0.10
BFO-MLP[11]	90.20	0.43
PRO-MLP[12]	91.50	0.31
HLOA-MLP[13]	91.30	0.23
HO-MLP[14]	90.40	0.38
LPO-MLP[15]	90.80	0.30
EEFO-MLP[16]	90.10	0.33
LEA-MLP[17]	90.80	0.22
NRBO-MLP[18]	90.40	0.53
FTTA-MLP[19]	90.10	0.71
BKA-MLP[20]	90.50	0.50
GO-MLP[21]	90.50	0.21

From Table 5, it is evident that the IHLOA-MLP algorithm continues to outperform the other 14 optimization algorithms, with the highest accuracy. Specifically, the accuracy of IHLOA-MLP is 3.6% higher than that of the MLP algorithm and 0.9% higher than that of the HLOA-MLP algorithm. Additionally, IHLOA-MLP has the smallest variance, indicating the best robustness. When compared to the dataset with feature vectors of current, voltage, temperature, and light intensity, the algorithm that is most affected among the 14 optimization algorithms is the MLP, with a decrease in accuracy of 2.55%. The algorithm least affected is the PRO-MLP, with a decrease in accuracy of 0.2%, and the IHLOA-MLP has a decrease in accuracy of 2.35%.

4.1.5 Voltage and light intensity are utilized as the input variable

From Table 6, it is evident that the IHLOA-MLP algorithm continues to outperform the other 14 optimization algorithms, with the highest accuracy. Specifically, the accuracy of IHLOA-MLP is 71.90%, which is 4.7% higher than that of the NRBO-MLP algorithm. Additionally, IHLOA-MLP has the smallest variance, indicating the best robustness. The ranking of the algorithms from highest to lowest accuracy is as follows: IHLOA-MLP, BFO-MLP, APO-MLP, HLOA-MLP, PRO-MLP, HO-MLP, LPO-MLP, EEFO-MLP, LEA-MLP, FTTA-MLP, BKA-MLP, GO-MLP, MLP. The ranking from lowest to highest variance is: IHLOA-MLP, BFO-MLP, APO-MLP, HLOA-MLP, PRO-MLP, HO-MLP, LPO-MLP, EEFO-MLP, LEA-MLP, FTTA-MLP, BKA-MLP, GO-MLP, MLP. The most unstable algorithm is the APO-MLP, with a variance of 0.41.

Table 6 Average recognition effect of each algorithm in the data set with voltage and light intensity as input

Algorithm	Accuracy(%)	Accuracy Variance
MLP[12]	68.70	0.24
APO-MLP[10]	68.70	0.41
IHLOA-MLP	71.90	0.13
BFO-MLP[11]	70.10	0.24
PRO-MLP[12]	68.50	0.18
HLOA-MLP[13]	70.10	0.15
HO-MLP[14]	68.40	0.15
LPO-MLP[15]	67.50	0.18
EEFO-MLP[16]	67.80	0.28
LEA-MLP[17]	68.50	0.26
NRBO-MLP[18]	67.20	0.25
FTTA-MLP[19]	69.00	0.15
BKA-MLP[20]	69.00	0.25
GO-MLP[21]	68.90	0.17

From Table 6, it is evident that the IHLOA-MLP algorithm continues to outperform the other 13 optimization algorithms, with the highest accuracy. Specifically, the accuracy of IHLOA-MLP is 3.2% higher

than that of the MLP algorithm and 1.8% higher than that of the HLOA-MLP algorithm. Additionally, IHLOA-MLP has the smallest variance, indicating the best robustness. When compared to the dataset with feature vectors of current, voltage, temperature, and light intensity, the algorithm that is most affected among the 14 optimization algorithms is the BKA-MLP, with a decrease in accuracy of 25.1%. The algorithm least affected is the BFO-MLP, with a decrease in accuracy of 21.5%, and the IHLOA-MLP has a decrease in accuracy of 22.65%.

4.1.6 Current and voltage are utilized as the input variables

From Table 7, it is evident that the IHLOA-MLP algorithm continues to outperform the other 14 optimization algorithms, with the highest accuracy. Specifically, the accuracy of IHLOA-MLP is 83.90%, which is 6.5% higher than that of the HO-MLP algorithm. Additionally, IHLOA-MLP has the smallest variance, indicating the best robustness. The ranking of the algorithms from highest to lowest accuracy is as follows: IHLOA-MLP, LPO-MLP, LEA-MLP, APO-MLP, BFO-MLP, NRBO-MLP, EEFO-MLP, HLOA-MLP, HO-MLP, FTTA-MLP, BKA-MLP, GO-MLP, MLP. The ranking from lowest to highest variance is: IHLOA-MLP, APO-MLP, LPO-MLP, BFO-MLP, LEA-MLP, HO-MLP, EEFO-MLP, PRO-MLP, NRBO-MLP, FTTA-MLP, BKA-MLP, GO-MLP, HLOA-MLP, MLP. The most unstable algorithm is the PRO-MLP, with a variance of 0.46.

From Table 7, it is evident that the IHLOA-MLP algorithm continues to outperform the other 13 optimization algorithms, with the highest accuracy. Specifically, the accuracy of IHLOA-MLP is 6.5% higher than that of the MLP algorithm and 5.8% higher than that of the HLOA-MLP algorithm. Additionally, IHLOA-MLP has the smallest variance, indicating the best robustness. When compared to the dataset with feature vectors of current, voltage, temperature, and light intensity, the algorithm that is most affected among the 14 optimization algorithms is the HLOA-MLP, with a decrease in accuracy of 15.9%. The algorithm least affected is the LEA-MLP, with a decrease in accuracy of 10.3%, and the IHLOA-MLP has a decrease in accuracy of 10.65%.

Table 7 shows the average recognition effect of each algorithm in the data set with current and voltage as input

Algorithm	Accuracy(%)	Accuracy Variance
MLP[12]	77.40	0.34
APO-MLP[10]	80.20	0.42
IHLOA -MLP	83.90	0.17
BFO-MLP[11]	79.30	0.30
PRO-MLP[12]	77.50	0.46
HLOA-MLP[13]	78.10	0.39
HO-MLP[14]	77.40	0.26
LPO-MLP[15]	80.80	0.33
EEFO-MLP[16]	80.50	0.32
LEA-MLP[17]	80.90	0.24
NRBO-MLP[18]	79.80	0.45
FTTA-MLP[19]	79.60	0.37
BKA-MLP[20]	80.30	0.38
GO-MLP[21]	77.90	0.26

4.1.7 Histogram of accuracy and variance

To evaluate the performance under different input conditions, we apply 14 algorithms to a dataset with variables such as current (C), voltage (V), temperature (T), and light intensity (L). Table 8 compares IHLOA-MLP with the best performing algorithm in each case. The histogram of accuracy and variance of various algorithms is shown in Figure 6.

Table 8 Average accuracy and variance of IHLOA-MLP and the optimal algorithm under different input features

Input Features	IHLOA-MLP		Best-Performing Algorithm	Best-Performing Algorithm	
	Accuracy(%)	Variance		Accuracy (%)	Variance
C、V、T、L	94.55	0.08	BKA-MLP[20]	94.10	0.12
V、C、L	86.40	0.41	BFO-MLP[11]	84.80	0.41
C、T、L	91.80	0.19	NRBO-MLP[18]	90.90	0.52
V、T、L	92.20	0.10	LEA-MLP[17]	90.80	0.22
V、L	71.90	0.13	HLOA-MLP[13]	70.10	0.15
C、V	83.90	0.17	LEA-MLP[17]	80.90	0.24

To evaluate the robustness of IHLOA-MLP under diverse environmental conditions, six kinds of input features are tested, including current (C), voltage (V), temperature (T), and light intensity (L). As shown in Table 8, IHLOA-MLP consistently outperformed 13 baseline algorithms (e. g., BKA-MLP, HLOA-MLP) in both accuracy and stability. For instance, with full input features (C, V, T, L), IHLOA-MLP achieves the highest accuracy of 94.55% (0.45% higher than BKA-MLP) and the lowest variance of 0.08, indicating superior resistance

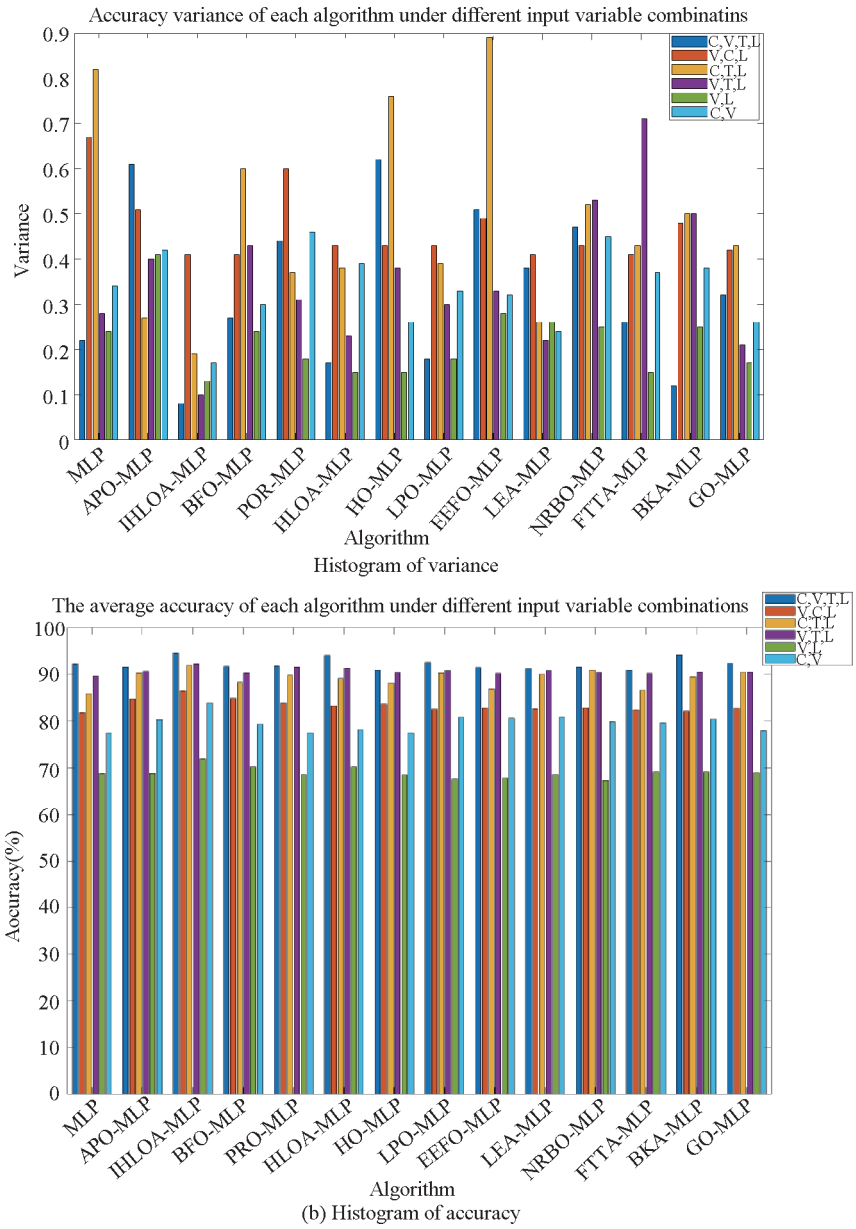

Fig.6 Accuracy and variance histogram

to environmental noise.

Notably, when input features are reduced, IHLOA-MLP exhibits smaller performance degradation compared to other algorithms. For example, using only voltage and light intensity, IHLOA-MLP's accuracy drops by 22.65%, whereas BKA-MLP suffered a 25.1% decline. This resilience is attributed to IHLOA's chaotic initialization and cross-strategy, which enhance feature adaptability. Figure 4 further visualizes the accuracy-variance trade-off across algorithms, demonstrating IHLOA-MLP's dominance in the Pareto front. In conclusion, experimental results show that IHLOA-MLP excels in both accuracy and stability. It achieves the highest accuracy and lowest variance in most cases. Notably, with V, T, and L as inputs, IHLOA-MLP attains higher accuracy with minimal input features, suggesting efficient operation with reduced data collection costs in practical applications.

4.2 Model Validation under Fault Data Input

The system is capable of identifying four common types of data: normal, open-circuit, shading, and short-circuit. To verify the monitoring performance of the newly proposed system on the target array, a continuous ten-day test was conducted. Each day, 80 data monitoring sessions were carried out in the morning and afternoon, covering 20 samples of each fault type, ultimately obtaining 1600 monitoring results. The specific monitoring results are shown in the confusion matrix as depicted in the figure below.

To validate the monitoring capabilities of the newly proposed system for the target array, a continuous ten-day test was conducted. Data monitoring was performed 80 times each in the morning and afternoon, encompassing 20 data instances for each of the various fault types, ultimately yielding 1600 monitoring results. The specific

monitoring outcomes are presented in the confusion matrix as depicted in the following figure.

According to the confusion matrix shown in Figure 7, the monitoring accuracy of the system is 88.81%. It is worth mentioning that there may be interference when switching fault types, leading to misjudgments. For example, when suddenly switching from a shading fault to an open-circuit fault, the voltage value will fluctuate, thereby affecting the accuracy of the open-circuit fault. Similarly, when suddenly switching to a short-circuit fault, the voltage value will also fluctuate. Additionally, when adjusting the light intensity, the temperature will change accordingly, but the DS18B20 cannot achieve an abrupt temperature change, instead showing a slowly rising trend, which may also lead to misjudgments. In practical applications, these interfering factors do not occur, and after eliminating these interferences, the system's accuracy is close to 90%. Although the IHLOA-MLP model has the potential for misjudgment, no misjudgments were observed in the fault display module of the upper computer's main interface. This is because the system is set to judge 3 times, and it is extremely rare for the same error type to appear continuously for 3 times. Through this strategy, the system successfully avoids being affected by the erroneous information brought about by model misjudgments, significantly enhancing the accuracy and reliability of the system's fault monitoring.

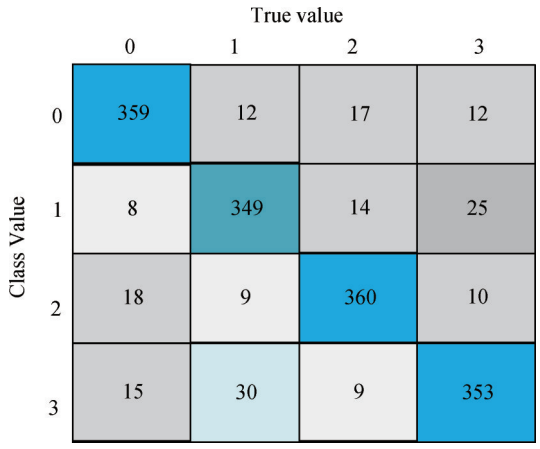

Fig.7 Confusion matrix of monitoring results

5 Conclusion

This study presents a comprehensive photovoltaic fault monitoring system that combines an STM32 microcontroller with the IHLOA-MLP algorithm. The hardware setup, featuring high-precision sensors like the BH1750 for light intensity, DS18B20 for temperature, and INA226 for current and voltage detection, along with the ESP8266 for wireless data transmission, ensures reliable and stable data acquisition. The software, developed in QT Creator, integrates the MLP model from OpenCV with the IHLOA algorithm, which draws inspiration from horned lizard survival strategies such as hiding, skin color change, blood squirting, and escaping, further enhanced by random walk and cross-matrix strategies. This integration optimizes the MLP model's weight and bias vectors, significantly improving fault monitoring accuracy and robustness.

The results highlight the IHLOA-MLP model's superior performance across various input parameters. It achieves the highest accuracy of 94.55% with the smallest variance when using current, voltage, temperature, and light intensity as inputs, demonstrating excellent stability and accuracy. Even with fewer input features, such as voltage and light intensity, the model maintains the highest accuracy of 71.90%, underscoring its adaptability and robustness.

Under different fault conditions, the system demonstrates its ability to accurately identify common photovoltaic fault types, including normal operation, open-circuit, shading, and short-circuit, with a monitoring accuracy of 88.81%. The introduction of an auxiliary monitoring mechanism based on consecutive judgment counts further enhances monitoring accuracy and reduces misjudgment risks.

While this study covers a range of photovoltaic fault types, future research will expand the system's fault coverage to include component aging, hot-spot effects, and performance declines due to environmental factors. This will involve validating the IHLOA framework on large-scale datasets from diverse industrial PV systems and generalizing the algorithm to optimize other machine learning models for broader fault scenarios. Additionally, efforts will focus on refining the hardware-software co-design to enhance energy efficiency and deployment scalability, ensuring the system's effectiveness in real-world applications.

Author Contribution:

Xiao Wenbo: Conceptualization, Writing - review & editing, Methodology, Funding acquisition; Dong Huangfeng: Data curation, Software, Validation, Writing-original draft; Wu Huaming: Methodology; Li Yongbo: Project administration;Liu Bin: Writing-review & editing.

Funding Information:

This work has been supported by the National Natural Science Foundation of China (12064027, and 12464010); 2022 Jiangxi Province High-level and High-skilled Leading Talent Training Project Selected (No. 63); Jiujiang "Xuncheng Talents" (No. JJXC2023032); Jiujiang Natural Science Foundation Project (Key Technologies Research on Autonomous Cruise Solar-Powered UAV-2025-1).

Data Availability:

The authors declare that the main data supporting the findings of this study are available within the paper and its Supplementary Information files.

Conflicts of Interest:

The authors declare no competing interests.

Dates:

Received 27 October 2024; Accepted 15 May 2025; Published online 30 June 2025

References

[1] Sayyad J, Nasikkar P. Design and development of low cost, portable, on-field IV curve tracer based on capacitor loading for high power rated solar photovoltaic modules[J]. *IEEE Access* , **2021**, 9: 70715-70731.

[2] Alami A H, Ramadan M, Abdelkareem M A, et al. Novel and practical photovoltaic applications[J]. *Thermal Science and Engineering Progress* , **2022**, 29: 101208.

[3] Mellit A, Tina G M, Kalogirou S A. Fault detection and diagnosis methods for photovoltaic systems: A review [J]. *Renewable & Sustainable Energy Reviews* , **2018**, 91: 1-17.

[4] Huang J M, Wai R J, Yang G J. Design of Hybrid Artificial Bee Colony Algorithm and Semi-Supervised Extreme Learning Machine for PV Fault Diagnoses by Considering Dust Impact [J]. *IEEE Transactions on Power Electronics* , **2020**, 35(7): 7086-99.

[5] Li B, Delpha C, Diallo D, et al. Application of artificial neural networks to photovoltaic fault detection and diagnosis: A review[J]. *Renewable and Sustainable Energy Reviews* , **2021**, 138: 110512.

[6] Aziz, Farkhanda, Azhar Ul Haq, et al. A novel convolutional neural network-based approach for fault classification in photovoltaic arrays[J]. *IEEE Access* ,**2020**, 8: 41889-41904.

[7] Hichri A, Hajji M, Mansouri M, et al. Genetic-Algorithm-Based Neural Network for Fault Detection and Diagnosis: Application to Grid-Connected Photovoltaic Systems [J]. *Sustainability* , **2022**, 14(17): 10518.

[8] Eldeghady G S, Kamal H A, Hassan M A M. Fault diagnosis for PV system using a deep learning optimized via PSO heuristic combination technique[J]. *Electrical Engineering* , **2023**: 1-15.

[9] Yu J, Liu Y. Research on Fault Diagnosis of Photovoltaic Array Based on ACA-RBF Neural Network Model[C].//2022 4th International Conference on Power and Energy Technology (ICPET). Beijing, China: IEEE, **2022**: 731-735.

[10] Wang, Kong, and Hisham A. Shehadeh. Artificial Protozoa Optimizer (APO): A novel bio-inspired metaheuristic algorithm for engineering optimization[J]. *Knowledge-Based Systems* , **2024**,295: 111737.

[11] Zareian, Lida, Javad Rahebi, and Mohammad Javad Shayegan. Bitterling fish optimization (BFO) algorithm[J]. *Multimedia Tools and Applications* , **2024**: 1-34.

[12] Taheri, Ahmad, Keyvan RahimiZadeh, et al. Partial reinforcement optimizer: An evolutionary optimization algorithm[J]. *Expert Systems with Applications* , **2024**, 238: 122070.

[13] Peraza-Vázquez, Hernán, Adrián Peña-Delgado, et al. A novel metaheuristic inspired by horned lizard defense tactics[J]. *Artificial Intelligence Review* , **2024**, 57(3): 59.

[14] Amiri M. H., Mehrabi Hash N., Montazeri M. Mirjalili,et al. Hippopotamus optimization algorithm: a novel nature-inspired optimization algorithm[J]. *Scientific Reports* , **2024**, 14(1): 5032.

[15] Ghasemi M., Zare M., Zahedi A., et al. Optimization based on performance of lungs in body: Lungs performance-based optimization (LPO) [J]. *Computer Methods in Applied Mechanics and Engineering* , **2024**, 419:116582.

[16] Zhao W., Wang L., Zhang Z., et al. Electric eel foraging optimization: A new bio-inspired optimizer for engineering applications[J]. *Expert Systems with Applications* , **2024**, 238: 122200.

[17] Yuansheng Gao, Jiahui Zhang, Yulin Wang, et al. Love Evolution Algorithm: a stimulus-value-role theory-inspired evolutionary algorithm for global optimization[J]. *The Journal of Supercomputing* , **2024**:1-62.

[18] Sowmya, Ravichandran, Manoharan Premkumar, Pradeep Jangir. Newton-Raphson-based optimizer: A new population-based metaheuristic algorithm for continuous optimization problems[J]. *Engineering Applications of Artificial Intelligence* , **2024**, 128: 107532.

[19] Tian, Zhirui, Mei Gai. Football team training algorithm: A novel sport-inspired meta-heuristic optimization algorithm for global optimization[J]. *Expert Systems with Applications* , **2024**, 245: 123088.

[20] Jun Wang, Wen-chuan Wang, X Hu, et al. Black-winged kite algorithm: a nature-inspired meta-heuristic for solving benchmark functions and engineering problems[J]. *Artificial Intelligence Review* , **2024**, 57(4): 1-53.

[21] Hamad, Rebwar Khalid, Tarik A. Rashid. GOOSE algorithm: a powerful optimization tool for real-world engineering challenges and beyond[J]. *Evolving Systems* , **2024**: 1-26.

[22] Rao S, Spanias A, Tepedelenlinoglu C. Solar array fault detection using neural networks [C]. 2019 IEEE international conference on industrial cyber physical systems (ICPS). IEEE, **2019**: 196-200.

[23] Arora S, Anand P. Chaotic grasshopper optimization algorithm for global optimization[J]. *Neural Computing and Applications* , **2019**, 31: 4385-4405.

[24] Song M. J., Jia H. M., Abualigah L., et al. Modified Harris Hawks Optimization Algorithm with Exploration Factor and Random Walk Strategy[J]. *Computational Intelligence and Neuroscience* , **2022**:4673665.

[25] Renxi Gong, Xianglong Li. A short-term load forecasting model based on crisscross grey wolf optimizer and dual-stage attention mechanism[J]. *Energies* , **2023**, 16(6): 2878.

[26] Satpathy P R, Aljafari B, Thanikanti S B, et al. Electrical fault tolerance of photovoltaic array configurations: Experimental investigation, performance analysis, monitoring and detection [J]. *Renewable Energy* , **2023**, 206: 960 – 981.

[27] Murugan M. S., David P. W., & Murugesan P. Analysis of voltage/current mismatch in solar photovoltaic power plants during fault panel replacement[J]. *Energy Sources, Part A: Recovery, Utilization, and Environmental Effects* , **2021**, 47 (1), 6510-6527.